minerals

MDPI

Article

Computational Insights into the Adsorption Mechanism of Zn Ion on the Surface (110) of Sphalerite from the Perspective of Hydration

Chenyang Zhang [1,2], Feng Zhang [1], Siyuan Liu [1], Dong Fan [3], Xin Rao [1], Jianhua Chen [4], Jing Wen [5], Yangge Zhu [2,*] and Wei Sun [1,*]

1 Hunan International Joint Research Center for Efficient and Clean Utilization of Critical Metal Mineral Resources, Key Laboratory of Hunan Province for Clean and Efficient Utilization of Strategic Calcium-Containing Mineral Resources, School of Minerals Processing and Bioengineering, Central South University, Changsha 410083, China; zhangchenyang@csu.edu.cn (C.Z.); 215611035@csu.edu.cn (F.Z.); 225612103@csu.edu.cn (S.L.); raoxin@csu.edu.cn (X.R.)

2 State Key Laboratory of Mineral Processing Science and Technology, BGRIMM Technology Group, Beijing 102628, China

3 Department of Chemistry, Key Laboratory of Environmentally Friendly Chemistry and Application of Ministry of Education, Xiangtan University, Xiangtan 411105, China; van_d17@163.com

4 School of Resources, Environment and Materials, Guangxi University, Nanning 530000, China; jhchen@gxu.edu.cn

5 Hubei Key Laboratory of Plasma Chemistry and Advanced Materials, School of Materials Science and Engineering, Wuhan Institute of Technology, Wuhan 430205, China; jing.wen@wit.edu.cn

* Correspondence: zhuyangge@bgrimm.com (Y.Z.); sunmenghu@csu.edu.cn (W.S.); Tel.: +86-010-59069507 (Y.Z.); +86-0731-8883-0482 (W.S.)

Abstract: Zn ions are widely reported to possess a depression effect on sphalerite in flotation. The effective adsorption of Zn ions on a sphalerite surface is critical to realize the inhibition effect. At the same time, zinc ions are easily hydrated in a slurry solution. Therefore, based on the first principle DFT calculation, the molecular mechanism of Zn ion adsorption on the surface of Sphalerite is further studied from the perspective of hydration. $[Zn(H_2O)_5]^{2+}$, $[Zn(OH)(H_2O)_3]^{+}$ and $[Zn(OH)_2(H_2O)_2]$ are found to be the effective components of Zn ions adsorbed on a sphalerite (110) surface in the neutral condition. Furthermore, the adsorption mechanism of $[Zn(H_2O)_5]^{2+}$ on a sphalerite (110) surface is mainly via the hybridization of Zn 3d orbital in the structure of $[Zn(H_2O)_5]^{2+}$ with surface S 3p orbitals. Additionally, the adsorption mechanism of $[Zn(OH)(H_2O)_3]^{+}$ and $[Zn(OH)_2(H_2O)_2]$ on a sphalerite (110) surface is primarily ascribed to the hybridization of surface Zn 3d orbital with O atom of hydroxyl ligand 2p orbitals. In addition, the H 1s orbits in the water molecules have a weaker interaction with the sphalerite surface S 3p orbits. This work sheds new light on the adsorption and inhibition mechanism of zinc ions on a sphalerite surface in a neutral aqueous solution.

Keywords: sphalerite; Zn ion; hydroxylation; hydration; DFT; depression mechanism

check for updates

Citation: Zhang, C.; Zhang, F.; Liu, S.; Fan, D.; Rao, X.; Chen, J.; Wen, J.; Zhu, Y.; Sun, W. Computational Insights into the Adsorption Mechanism of Zn Ion on the Surface (110) of Sphalerite from the Perspective of Hydration. *Minerals* **2023**, *13*, 1113. https://doi.org/10.3390/min13091113

Academic Editor: Elvis Fosso-Kankeu

Received: 12 July 2023
Revised: 31 July 2023
Accepted: 3 August 2023
Published: 23 August 2023

Copyright: © 2023 by the authors. Licensee MDPI, Basel, Switzerland. This article is an open access article distributed under the terms and conditions of the Creative Commons Attribution (CC BY) license (https://creativecommons.org/licenses/by/4.0/).

1. Introduction

Metal ions have a profound influence on the flotation behavior of minerals [1–4]. Some can activate mineral flotation, and some can inhibit mineral flotation; their flotation performance mainly depends on the type, radius, valence, and concentration of metal ions [2,5]. The role of metal ions in the flotation process is related to the environment of the flotation solution, especially the pH value of the pulp [6–9]. Under acidic conditions, metal ions mainly exist in the form of free ions. With the increase in pH value of the solution, metal ions will be gradually hydrated and even undergo hydroxylation. Therefore, the hydration (hydroxylation) has an important influence on the adsorption behavior of metal ions on a mineral surface [10,11].

In the flotation separation of sulfide minerals, zinc ions are most commonly used as sphalerite depressor components. For example, Jian Liu et al. found that sphalerite was significantly selectively depressed by the combination of zinc sulfate ($ZnSO_4$) and sodium dimethyl dithiocarbamate (SDD), but chalcopyrite was just slightly depressed [12]. They also explained that the performance of the combined depressant only depended on the pH value of the flotation medium and the dosage of the reagent [12]. In addition, Yanfang Cui reported that the selective inhibition effect of $ZnSO_4$ + SDD on sphalerite was better than that of $ZnSO_4$ or SDD alone in the Pb–Zn sulfide mineral flotation system [13]. Zhicong Wei et al. studied the selective depression mechanism of sphalerite of combination depressant $K_3[Fe(CN)_6]$, $ZnSO_4$, and Na_2CO_3 in Pb–Zn sulfide mineral flotation separation [14]. They found that, when the dosages of $K_3[Fe(CN)_6]$, $ZnSO_4$, and Na_2CO_3 were 1.8×10^{-5} mol/L, 8×10^{-5} mol/L, and 2.4×10^{-4} mol/L, respectively, the recovery of galena was 92.56%, while that of sphalerite (Pb^{2+} activation) was only 7.65%. Qian Wei et al. developed a low-alkaline and non-desliming process which could lower production costs and reduce environmental pollution [15]. In this new flotation approach, collector WS (a mixture of ethyl thiocarbamate, ammonium dibutyldithiophosphate, and dithiophosphate-25) combined with depressant Na_2S, $ZnSO_4$, and Na_2SO_3 were used for Pb–S flotation to avoid a high-alkaline process. From the above research progress, it can be seen that zinc ions are an important component of sphalerite combined depressants.

During the depression process, zinc ions will undergo hydroxylation and hydration, which will affect the depression process of zinc ions on the surface of sphalerite. Therefore, the hydroxylation and hydration of zinc ions should be fully considered in the flotation process of sphalerite in order to more accurately study the interaction mechanism between zinc ions and sphalerite surface [10,16,17]. So far, few papers have systematically reported the depression mechanism of zinc ions on the surface hydroxylation and hydration of sphalerite. The effect of hydroxylation and hydration on zinc ion inhibition of sphalerite remains unclear.

Due to the remarkable development of computational quantum chemistry, the molecular mechanism of interfacial interaction of metal ions in flotation can be studied more systematically and deeply. For instance, Anruo Luo et al. studied the mechanism of the hydroxylation and hydration of Ca^{2+}, Fe^{3+}, Cu^{2+}, and Pb^{2+} ions on the surface of quartz based on DFT calculations [10]. Yuanjia Luo et al. investigated the adsorption performance and mechanism of hydrated Ca^{2+} on a talc (001) basal surface using DFT calculations [17]. Jian Liu et al. indicated that the presence of water molecules on a sphalerite surface was detrimental to SDD and BX attachment on the sphalerite surface based on DFT calculations [18]. Accordingly, the influence mechanism of hydroxylation and hydration on the adsorption of zinc ions on a sphalerite surface was investigated through the first-principle DFT calculations, which helps us to better understand the hydroxylation and hydration of zinc ions in a neutral flotation solution and how it affects the adsorption of zinc ions on the surface of zinc ores.

2. Computational Models and Methods

All the DFT calculations were performed by using CASTEP module in the Materials Studio 2017 package [19]. The original crystal cell structure of sphalerite used were acquired from the American Mineralogist Crystal Structure Database [20]. The approximation of the exchange-correlation potential of the Generalized Gradient Approximation (GGA) is performed with the PW91 functional [21]. The interaction between valence electrons and ionic nuclei was described with ultrasoft pseudopotential. The convergence threshold of self-consistent field interaction is 1×10^{-6} eV/atom. Energy, maximum force, maximum stress, and maximum displacement had convergence tolerances of 1×10^{-5} eV/atom, 0.03 eV/Å, 0.05 Gpa, and 1×10^{-3} Å, respectively. For the geometry optimization of original crystal cell, a cutoff energy of 400 eV and k-point meshes of $4 \times 4 \times 4$ were utilized in accordance with the Monkhorst–Pack method. In order to accurately describe the weak

interaction of dispersion, DFT-D correction using the Tkatchenko–Scheffler (TS) method was also used in all calculations [22,23].

The sphalerite (110) surface was reported to be the most stable surface in thermodynamics [24–26]. Therefore, the slab model of the (110) crystal surface was cut out and finally amplified into a 3×2×1 supercell model. Then, a slab model of sphalerite (110) surface with three layers of thickness and 25 Å vacuum layer was constructed. As is shown in Figure 1, the slab model of sphalerite (110) surface has obvious relaxation, and sulfur sites in the surface are more prominent after optimization. The water molecule and the structures of hydroxylation and hydration of the Zn ion were pre-optimized in a cubic cell of 20 × 20 × 20 $Å^3$ using the k-point of Gamma. For the surface model calculation, k-point was set as 2 × 2 × 1. The configurations of valence electrons of Zn, S, H, and O were performed as $3d^{10}4s^2$, $3s^23p^4$, H-$1s^1$, and O-$2s^22p^4$, respectively.

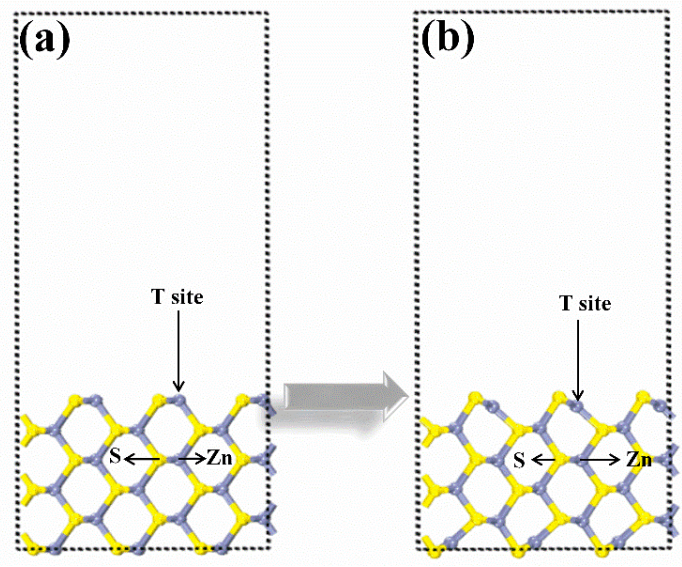


Figure 1. Slab (110) model of sphalerite: (**a**) before optimization, (**b**) after optimization.

The stability of hydrated structures of Zn ions can be described with the adsorption energy value (ΔE_{ad}) and successive water molecule adsorption energy value (ΔE_{sad}), which could be calculated with Equations (1) and (2), respectively [17]:

$$\Delta E_{ad} = E[M(H_2O)_N] - E(M) - N \times E(H_2O) \quad (1)$$

$$\Delta E_{sad} = E[M(H_2O)_{N+1}] - E[M(H_2O)_N] - E(H_2O) \quad (2)$$

where M denotes the primary component of the Zn ion, and N denotes the coordinate number of H_2O. $E[M(H_2O)_{N+1}]$ and $E[M(H_2O)_N]$ denote the calculated energy values of $M(H_2O)_{N+1}$ and $M(H_2O)_N$, respectively; E(M) represents the calculated energy value of Zn^{2+}; $E(H_2O)$ represents the calculated energy value of H_2O. The larger the negative value of ΔE_{ad}, the more stable the hydration configuration. Similarly, the greater the negative value of ΔE_{sad}, the easier the successive adsorption of H_2O is.

The adsorption energy value can be used to evaluate the adsorption performance of different adsorbates on the mineral surface, and its definition is as follows [27,28]:

$$E_{ads} = E(total) - E(slab) - E(adsorbate) \quad (3)$$

where E(total) is the total energy value of the system of the slab model with the hydrated Zn ion adsorbed. E(slab) and E(adsorbate) are the energy values of the slab model and hydrated Zn ion, respectively.

3. Results and Discussion

3.1. Effective Hydrated Components of Zn Ion

According to the chemical theory of flotation solution, there are three main components of the Zn ion in the neutral solution, including Zn^{2+}, $[Zn(OH)]^{+}$, and $Zn(OH)_2$ [6,29]. In addition, the flotation process is carried out in an aqueous environment, where zinc ions coordinate with water molecules to form a hydrated structure. The hydration structure of Zn^{2+}, $[Zn(OH)]^{+}$ and $Zn(OH)_2$ should have the corresponding most stable configuration, so it is necessary to study these most stable hydration structures first.

Table S2 presents the structural parameters, adsorption energies (ΔE_{ad}), and successive water adsorption energies (ΔE_{sad}) of $[Zn(H_2O)_{1-8}]^{2+}$, $[Zn(OH)(H_2O)_{1-5}]^{+}$, and $[Zn(OH)_2(H_2O)_{1-4}]$. The optimized structures of $[Zn(H_2O)_{1-8}]^{2+}$, $[Zn(OH)(H_2O)_{1-5}]^{+}$, and $[Zn(OH)_2(H_2O)_{1-4}]$ are shown in Figure 2, Figure 3, and Figure 4, respectively. For Zn^{2+}, when the coordination number of water molecules increases from one tosix, ΔEad gradually decreases, and ΔEsad gradually increases. When the number of H_2O ligands reached 7, ΔE_{sad} reached a relatively high value (−100.8 kJ/mol). According to Figure 2, the optimization results of the coordination structures of water molecules and zinc ions show that the coordination adsorption configurations of one and five water molecules with zinc ions are unidirectional. The adsorbed water molecules are distributed in the same hemisphere space as the zinc ions, which is consistent with the previous literature conclusions [30]. When the number of water molecules in the coordination reaches six, the adsorption mode becomes omnidirectional adsorption, with Zn^{2+} located in the center and surrounded by six water molecules. In addition, when the number of water molecules adsorbed by the coordination exceeds six, the structure of the hydrated Zn^{2+} complex becomes unstable. When the seventh water molecule is adsorbed, the bond length of Zn–O is 3.8293 Å, which is much longer than the average bond length of Zn–O (2.1146 Å). When the eighth water molecule is adsorbed, the bond length of the newly formed Zn–O bond is also much longer than the average bond length of Zn–O. Therefore, the most stable hydration configuration of Zn^{2+} is the coordination structure with six water molecules [31].

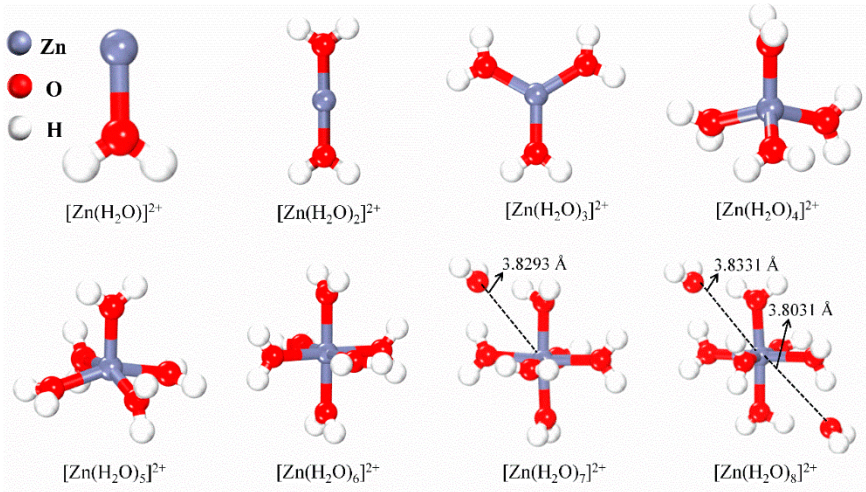


Figure 2. Optimized geometries of $[Zn(H_2O)_{1-8}]^{2+}$.

For $[Zn(OH)]^{+}$, as presented in Table S2, the ΔE_{ad} is gradually decreased and ΔE_{sad} is gradually increased when the number of H_2O ligands increases from one to three. When the number of H_2O ligands reached four, ΔE_{sad} reached a maximum value (71.2 kJ/mol). As shown in Figure 3, when $[Zn(OH)]^{+}$ adsorbs three water molecules through coordination, it forms a tetrahedral-like structure. When the fourth water molecule is adsorbed, the Zn–O bond length is 3.3084 Å, which is much greater than the average bond length of Zn–O (2.3294 Å). When the fifth water molecule is adsorbed, the bond length of the newly formed Zn–O bond is also much longer than the average Zn–O bond length, indicating

that the bonding between Zn and the O atoms in the fourth and fifth H_2O is not significant. Therefore, under the condition of the selected calculation parameters, the maximum number of water molecules in the first hydration layer of $[Zn(OH)]^+$ is three, which is the most stable hydration configuration of $[Zn(OH)]^+$.

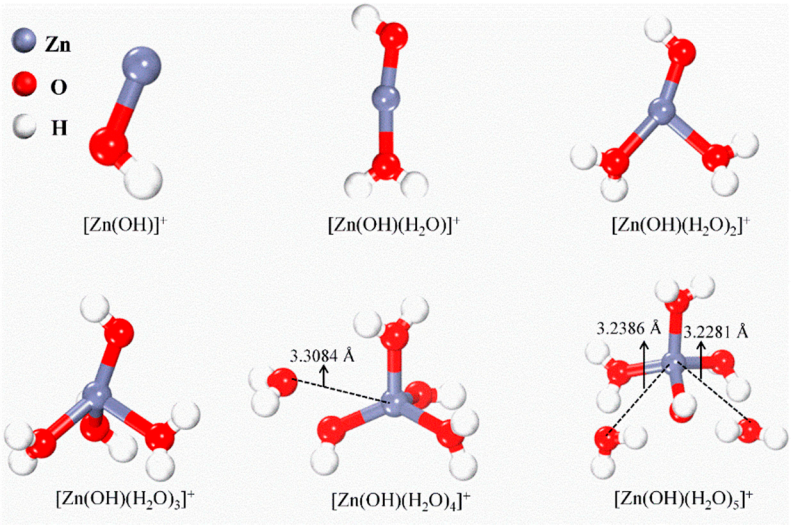


Figure 3. Optimized geometries of $[Zn(OH)(H_2O)_{1–5}]^+$.

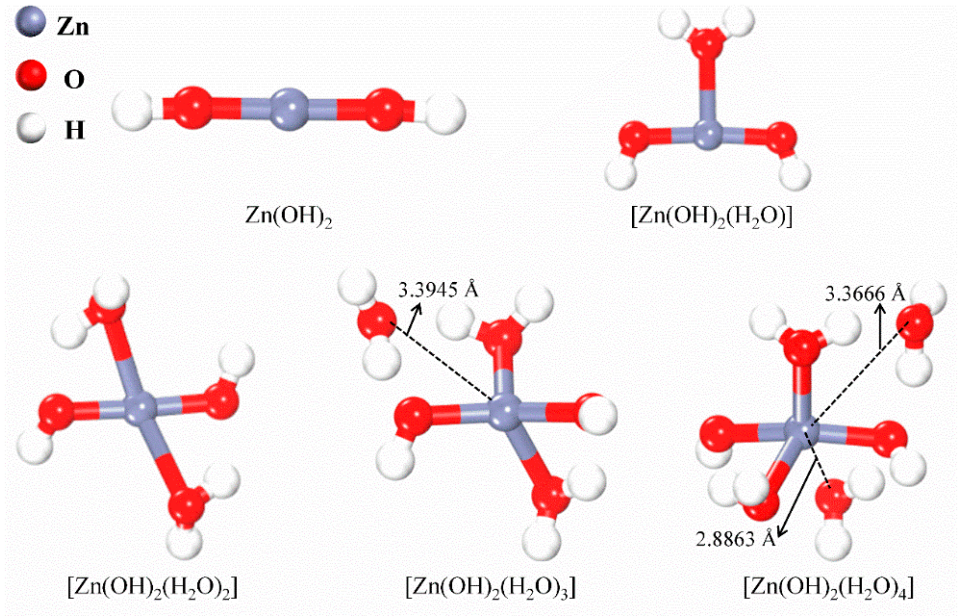


Figure 4. Optimized geometries of $[Zn(OH)_2(H_2O)_{1–5}]$.

Under high alkalinity conditions, zinc ions mainly exist in the form of Zn $(OH)_2$. In fact, under neutral conditions, Zn $(OH)_2$ is also one of the main components of zinc ions. It can be seen from Table S2 that the ΔE_{ad} is also gradually decreased when the number of H_2O ligands increase from one to four. As shown in Figure 4, $Zn(OH)_2$ can adsorb two water molecules at most. When water molecules continue to be adsorbed on $[Zn(OH)_2(H_2O)_2]$, the distance between the Zn atom and the O atom in the third water is much greater than the distance between the initial two water molecules and the zinc atom. When the fourth water molecule continues to be adsorbed on $[Zn(OH)_2(H_2O)_3]$, the water molecule will also be far away from the zinc atom, indicating that the most stable hydration configuration of $Zn(OH)_2$ is $[Zn(OH)_2(H_2O)_2]$.

According to the periodic model calculations, the most stable hydration configurations of Zn^{2+}, $[Zn(OH)]^+$, and $Zn(OH)_2$ were obtained through the above bond length and energy analysis. Furthermore, the results of effective hydrated components of Zn ion were further calculated with cluster model calculations and are presented in the Supplementary Materials, which are consistent with the results of the periodic model [32,33]. Therefore, the adsorption behaviors and bonding mechanisms of $[Zn(H_2O)_6]^{2+}$, $[Zn(OH)(H_2O)_3]^+$, and $[Zn(OH)_2(H_2O)_2]$ on a sphalerite (110) surface were further investigated under neutral conditions.

3.2. Adsorption Configurations of Zinc Ions on Sphalerite Surface

In order to better understand the effect of hydration of Zn ions on mineral surface adsorption, the adsorption configurations of Zn ions without and with hydration are shown in Figures 5 and 6, respectively. The corresponding adsorption energy values of Zn^{2+}, $[Zn(OH)]^+$, and $[Zn(OH)_2]$ on the sphalerite (110) surface are presented in Table S3. Figure 5a gives a sphalerite (110) surface view. The S and Zn atoms at the top position have unsaturated residual bonding abilities. As shown in Figure 5b, Zn^{2+} is adsorbed on the S_7 site in the mineral surface with a distance of 3.084 Å between the $Zn_{b\text{-}1}$ and S_7 atoms, and their adsorption energy is −17.4 kJ/mol, which indicates that the Zn atom is not sulfophilic [34]. Figure 5c shows the adsorption configuration of $[Zn(OH)]^+$. The $[Zn(OH)]^+$ is adsorbed on the sphalerite through the $Zn_{c\text{-}1}$–S_5 and $O_{c\text{-}1}$–Zn_6 bonds. The corresponding bond lengths of $Zn_{c\text{-}1}$–S_5 and $O_{c\text{-}1}$–Zn_6 are 2.108 and 2.043 Å, respectively. The adsorption energy of $[Zn(OH)]^+$ on the sphalerite (110) surface is −158.6 kJ/mol. As presented in Figure 5d, the adsorbate of $[Zn(OH)_2]$ will interact with Zn_6, Zn_5, and S_5 atoms on the sphalerite (110) surface to form $O_{d\text{-}1}$–Zn_6, $O_{d\text{-}2}$–Zn_5, and $Zn_{d\text{-}1}$–S_5 bonds. The bond lengths of $O_{d\text{-}1}$–Zn_6, $O_{d\text{-}2}$–Zn_5, and $Zn_{d\text{-}1}$–S_5 are 2.056, 2.055, and 3.718 Å, respectively. In addition, the adsorption energy of $[Zn(OH)_2]$ on the sphalerite (110) surface is −231.0 kJ/mol.

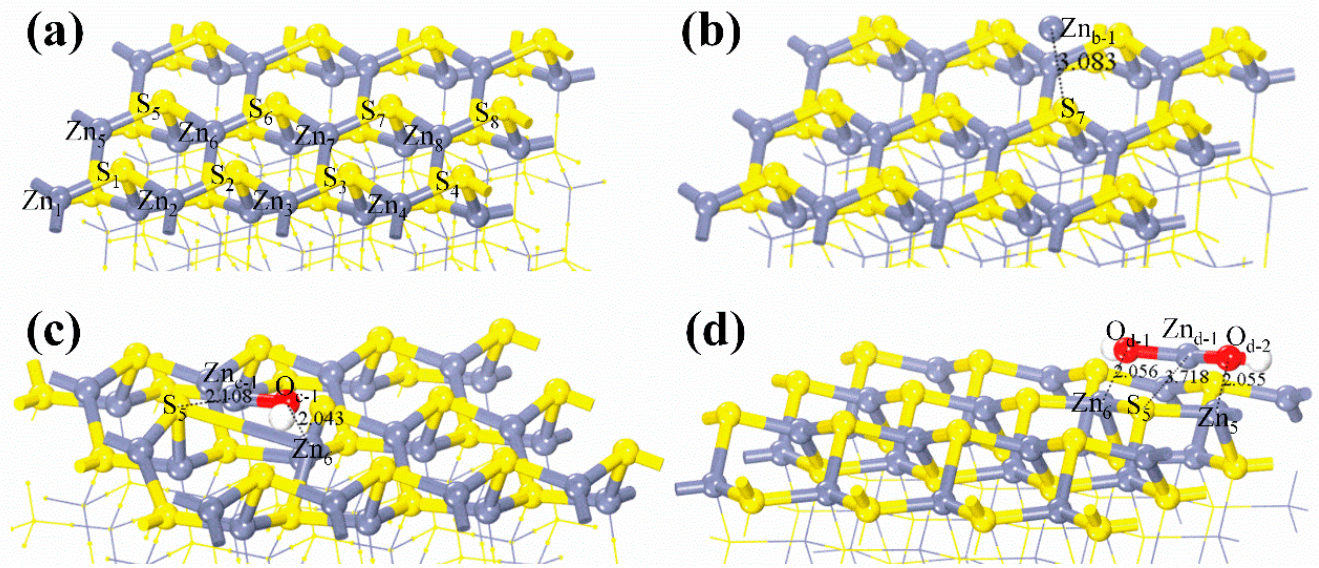


Figure 5. Adsorption configuration without hydration of Zn ion: (**a**) sphalerite (110) surface, (**b**) Zn^{2+} adsorption configuration, (**c**) $[Zn(OH)]^+$ adsorption configuration, (**d**) $Zn(OH)_2$ adsorption configuration.

Figure 6 shows the adsorption configuration of Zn ions with hydration on a sphalerite (110) surface. The corresponding adsorption energy values of $[Zn(H_2O)_5]^{2+}$, $[Zn(OH)(H_2O)_3]^+$, and $[Zn(OH)_2(H_2O)_2]$ on the sphalerite (110) surface are presented in Table S4. It should be emphasized that the adsorption of water molecules on the surface of sphalerite is relatively weak, only 60.6 kJ/mole, and this work mainly studies the adsorption of hydrated zinc ions in a neutral pulp aqueous solution on the surface of sphalerite, so the hydration and hydroxylation of the surface of sphalerite are not considered.

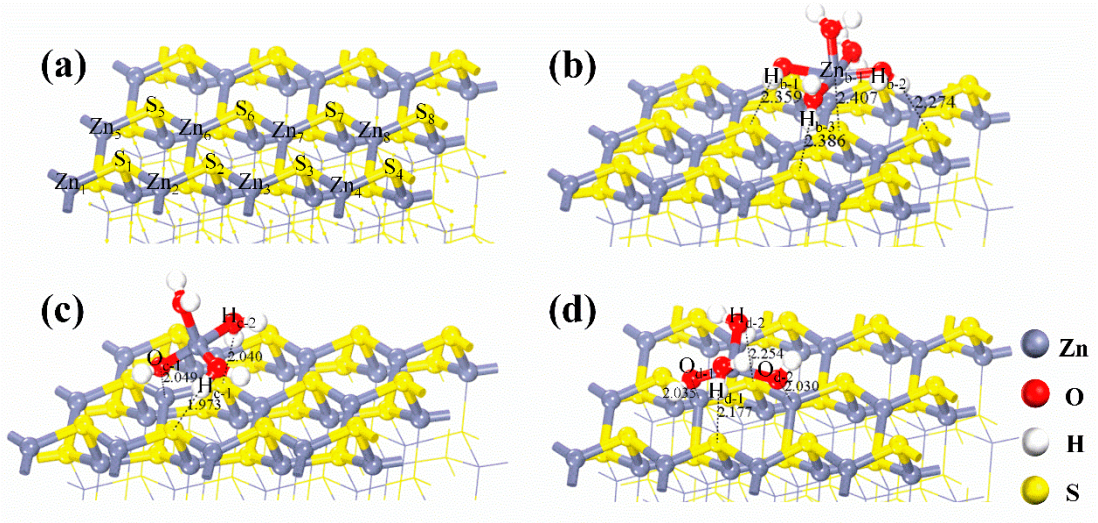


Figure 6. (**a**) Sphalerite (110) surface view; (**b**) $[Zn(H_2O)_5]^{2+}$ adsorption configuration, (**c**) $[Zn(OH)(H_2O)_3]^{+}$ adsorption configuration, and (**d**) $[Zn(OH)_2(H_2O)_2]$ adsorption configuration on sphalerite (110) surface.

The coordination structure of Zn^{2+} with six water molecules has been proved to be the most stable. However, the interaction between Zn^{2+} coordinated by six water molecules and the surface of sphalerite is a weak hydrogen–sulfur bond. The hydrogen–sulfur bond is relatively weak, resulting in the unstable adsorption configuration of $[Zn(H_2O)_6]^{2+}$ on the sphalerite surface. After many tests, the structure of $[Zn(H_2O)_5]^{2+}$ was found to be the most favorable adsorption configuration on the surface of sphalerite (110). Figure 6b illustrates the adsorption configuration of $[Zn(H_2O)_5]^{2+}$ on the sphalerite (110) surface. The adsorbate of $[Zn(H_2O)_5]^{2+}$ could be adsorbed on the S_6, S_3, S_7, and S_8 sites, forming $H_{b\text{-}1}$–S_6, $H_{b\text{-}3}$–S_3, $H_{b\text{-}2}$–S_8, and $Zn_{b\text{-}1}$–S_7 bonds. The bond lengths of $H_{b\text{-}1}$–S_6, $H_{b\text{-}3}$–S_3, $H_{b\text{-}2}$–S_8, and $Zn_{b\text{-}1}$–S_7 are 2.359, 2.386, 2.274, and 2.407 Å, respectively. The adsorption energy value of $[Zn(H_2O)_5]^{2+}$ on the sphalerite (110) surface is −144.5 kJ/mol. Figure 6c displays the adsorption configuration of $[Zn(OH)(H_2O)_3]^{+}$ on the sphalerite (110) surface. $[Zn(OH)(H_2O)_3]^{+}$ is adsorbed on the sphalerite surface through $O_{c\text{-}1}$–Zn_6, $H_{c\text{-}1}$–S_2, and $H_{c\text{-}2}$–S_6 bonds. The corresponding bond lengths of $O_{c\text{-}1}$–Zn_6, $H_{c\text{-}1}$–S_2, and $H_{c\text{-}2}$–S_6 are 2.049, 1.973, and 2.040 Å, respectively. The adsorption energy value of $[Zn(OH)(H_2O)_3]^{+}$ on the sphalerite (110) surface is –177.1 kJ/mol. Figure 6d represents the adsorption configuration of $[Zn(OH)_2(H_2O)_2]$ on the sphalerite (110) surface. As shown in Figure 5d, the $O_{d\text{-}1}$, $O_{d\text{-}2}$, $H_{d\text{-}1}$, and $H_{d\text{-}2}$ atoms in $[Zn(OH)_2(H_2O)_2]$ are coordinated with Zn_6, Zn_7, S_2, and S_6 atoms in the sphalerite (110) surface to form $O_{d\text{-}1}$–Zn_6, $O_{d\text{-}2}$–Zn_7, $H_{d\text{-}1}$–S_2, and $H_{d\text{-}2}$–S_6 bonds. The bond lengths of $O_{d\text{-}1}$–Zn_6, $O_{d\text{-}2}$–Zn_7, $H_{d\text{-}1}$–S_2, and $H_{d\text{-}2}$–S_6 bonds are 2.035, 2.030, 2.177, and 2.254 Å, respectively. The adsorption energy value of $[Zn(OH)_2(H_2O)_2]$ on the sphalerite (110) surface is −237.5 kJ/mol.

According to Table S3, the adsorption energy values of Zn^{2+}, $[Zn(OH)]^{+}$, and $[Zn(OH)_2]$ on the sphalerite (110) surface are −17.4, −158.6, and −231.0 kJ/mol, respectively. After hydration, the adsorption energy values of $[Zn(H_2O)_5]^{2+}$, $[Zn(OH)(H_2O)_3]^{+}$, and $[Zn(OH)_2(H_2O)_2]$ on the sphalerite (110) surface presented in Table S4 are −144.5, −177.1, and −237.5 kJ/mol, respectively. It could be found that hydration significantly promotes the adsorption of Zn^{2+}, $[Zn(OH)]^{+}$, and $[Zn(OH)_2]$ on the surface of sphalerite (110), especially the adsorption of Zn^{2+}. The adsorption energy value of $[Zn(H_2O)_5]^{2+}$ on sphalerite (110) surface is much lower than that of Zn^{2+}. The adsorption energy value of $[Zn(OH)_2(H_2O)_2]$ on sphalerite (110) surface is the lowest, indicating that the adsorption of $[Zn(OH)_2(H_2O)_2]$ is the most stable, which is consistent with the experimental result showing that the depression effect of Zn ion on sphalerite increases with the increase in pH [3,13]. When $Zn(OH)_2(H_2O)_2]$ is adsorbed on the sphalerite (110) surface, the two oxygen atoms of the hydroxyl ligand in the structure of $[Zn(OH)_2(H_2O)_2]$ occupy the zinc sites in the surface of the sphalerite. Additionally, an

oxygen atom of the hydroxyl ligand in the structure of $[Zn(OH)(H_2O)_3]^+$ also occupies a zinc site. For the adsorption of $[Zn(H_2O)_5]^{2+}$, there are no atoms in $[Zn(H_2O)_5]^{2+}$ occupying the zinc sites of the sphalerite surface. Therefore, the depression effect of zinc ions is not ideal under acidic conditions. The zinc site in the surface of sphalerite is the active site adsorbed by the collector. When the zinc sites are occupied by the oxygen atoms of the hydroxyl ligand in the structure of $[Zn(OH)(H_2O)_3]^+$ and $[Zn(OH)_2(H_2O)_2]$, it is difficult for the collector to be adsorbed on the zinc site in the sphalerite surface effectively.

3.3. Hirshfeld Charge Population Analysis

Charge population is an effective method to directly characterize the electron distribution and provides a simple and effective method to describe the charge transfer between different atoms. Hirshfeld charge populations of bonding atoms before and after the adsorption of hydrated Zn ions are shown in Table S5.

When the $[Zn(H_2O)_5]^{2+}$ is adsorbed on the sphalerite (110) surface, the net electrons of the $H_{b\text{-}1}$, $H_{b\text{-}2}$, and $H_{b\text{-}3}$ atoms decrease from 0.11 e to −0.10 e, 0.12 e to 0.10 e, and 0.14 e to 0.09 e, respectively. Furthermore, the atom of S_6 bonded to $H_{b\text{-}1}$ increases from −0.30 e to −0.27 e. The net electrons of the S_8 and S_3 atoms on the surface increase from −0.27 e to −0.26 e. The atom in the $Zn_{b\text{-}1}$–S_7 bond also changes. The net electrons of $Zn_{b\text{-}1}$ atoms decrease from 0.40 e to 0.39 e. The net electrons of S_7 atoms increase from −0.27 e to −0.24 e. These results indicated that the atoms in structure of $[Zn(H_2O)_5]^{2+}$ have weak interactions with the sphalerite surface.

When the $[Zn(OH)(H_2O)_3]^+$ is adsorbed on the sphalerite (110) surface, the net electrons of the $O_{c\text{-}1}$ increase from −0.42 e to −0.32 e and the atom of Zn_6 decreases from 0.31 e to 0.26 e, which indicate that the $O_{c\text{-}1}$ atom and the Zn_6 atom have a strong interaction. Furthermore, the net electrons of $H_{c\text{-}1}$ and $H_{c\text{-}2}$ decrease from 0.18 e to 0.07 e and 0.18 e to 0.09 e. The net electrons of S_2 bonded to $H_{c\text{-}1}$ increase from −0.31 e to −0.24 e. In addition, the net electrons of S_6 bonded to $H_{c\text{-}2}$ increase from −0.30 e to −0.25 e. These results illustrate that the atoms of $H_{c\text{-}1}$ and $H_{c\text{-}2}$ in the adsorbate of $[Zn(OH)(H_2O)_3]^+$ have a weak interaction with the sulfur atoms on the surface of the sphalerite.

When the $[Zn(OH)_2(H_2O)_2]$ is adsorbed on the sphalerite (110) surface, the net electrons of surface Zn_6 atom decrease by 0.07 e from 0.31 to 0.24 e. Those of the $O_{d\text{-}1}$ bonded to Zn_6 increase by 0.12 e from −0.44 e to −0.32 e. In addition, the net electrons of the surface Zn_7 atom decrease by 0.07 e from 0.31 to 0.24 e. Those of the $O_{d\text{-}2}$ bonded to the Zn_7 increase by 0.12 e from −0.43 e to −0.31 e. It can be seen that the oxygen in the structure of $[Zn(OH)_2(H_2O)_2]$ will be strongly adsorbed on the surface Zn site, preventing the interaction of the collector with the surface of the sphalerite. The net electrons of $H_{d\text{-}1}$ and $H_{d\text{-}2}$ decrease from 0.18 e to 0.10 e and 0.18 e to 0.11 e. The net electrons of the corresponding bonding S_2 increase from −0.30 e to −0.24 e. Additionally, the net electrons of the S_6 increase from −0.29 e to −0.28 e. It also can be inferred that there is weak interaction between the hydrogen atoms of $H_{d\text{-}1}$ and $H_{d\text{-}2}$ in the $[Zn(OH)_2(H_2O)_2]$ and the surface sulfur atoms. Through the analysis of charge population, we can more clearly and intuitively obtain the change of charge before and after the adsorption of hydrated Zn ion on the surface of the sphalerite. To further investigate the interaction between hydrated Zn ion and the sphalerite surface, an electron density of different adsorbates adsorbed on the surface of sphalerite is shown in Figure 7. The results in Figure 7 are consistent with the Hirshfeld charge population results described above.

3.4. Bond Population Analysis

The Mulliken bond population analysis is utilized to determine the strength and weakness of covalence. When the bond population is larger, it indicates that the bond's covalency is stronger [35]. As shown in Table S6, the bond populations of clearly bonded atoms are investigated to further understand the bonding adsorption properties of $[Zn(H_2O)_5]^{2+}$, $[Zn(OH)(H_2O)_3]^+$, and $[Zn(OH)_2(H_2O)_2]$ on the sphalerite (110) surface.

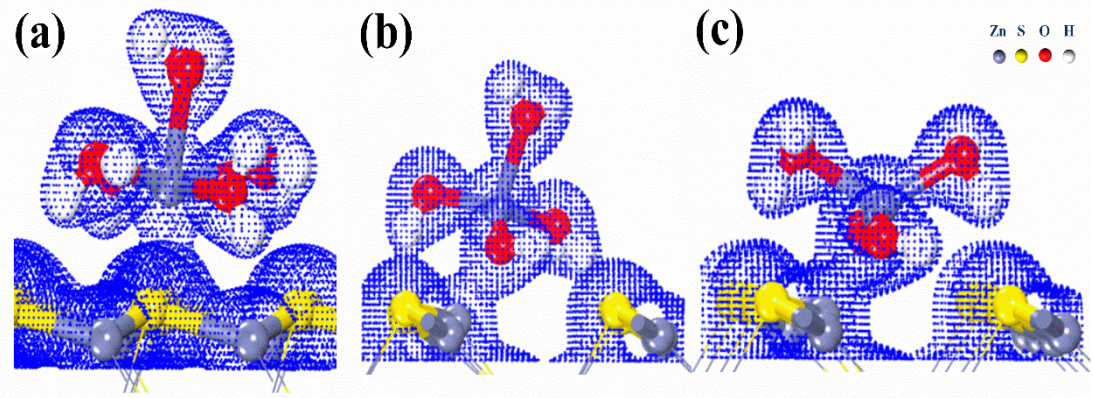


Figure 7. Electron density of different adsorbates adsorbed on the surface of sphalerite: (**a**) $[Zn(H_2O)_5]^{2+}$, (**b**) $[Zn(OH)(H_2O)_3]^{+}$, (**c**) $[Zn(OH)_2(H_2O)_2]$ (isovalue = 0.25).

When the $[Zn(H_2O)_5]^{2+}$ was adsorbed on the sphalerite (110) surface, the bond populations of $H_{b\text{-}1}$–S_6, $H_{b\text{-}2}$–S_8, and $H_{b\text{-}3}$–S_3 is 0.06, 0.07, and 0.07, respectively, which demonstrated that the $H_{b\text{-}1}$–S_6, $H_{b\text{-}2}$–S_8, and $H_{b\text{-}3}$–S_3 bonds had weak covalency. However, the bond population of $Zn_{b\text{-}1}$–S_7 was 0.30, showing that the bond of $Zn_{b\text{-}1}$–S_7 had strong covalency. When the $[Zn(OH)(H_2O)_3]^{+}$ was adsorbed on the sphalerite (110) surface, the bond population of $O_{c\text{-}1}$–Zn_6 was 0.29, indicating that the bond of $O_{c\text{-}1}$–Zn_6 had strong covalency. The bond populations of $H_{c\text{-}1}$–S_2 and $H_{c\text{-}2}$–S_6 were 0.17 and 0.15, which indicated a weak covalent interaction of $H_{c\text{-}1}$–S_2 and $H_{c\text{-}2}$–S_6. When the $[Zn(OH)_2(H_2O)_2]$ was adsorbed on the sphalerite (110) surface, the bond populations of $O_{d\text{-}1}$–Zn_6 and $O_{d\text{-}2}$–Zn_7 were both 0.31. This indicated that both $O_{d\text{-}1}$–Zn_6 and $O_{d\text{-}2}$–Zn_7 bonds had strong covalence. Nevertheless, the bond populations of $H_{d\text{-}1}$–S_2 and $H_{d\text{-}2}$–S_6 were 0.11 and 0.09, which indicated that the $H_{d\text{-}1}$–S_2 and $H_{d\text{-}2}$–S_6 bonds had strong ionicity and weak covalency. According to the analysis of bond population, it could be concluded that the surface Zn sites were strongly occupied by the O atom of the hydroxyl ligand in the structure of $[Zn(OH)(H_2O)_3]^{+}$ and $[Zn(OH)_2(H_2O)_2]$, resulting in the depression of sphalerite.

3.5. PDOS Analysis

In order to further explain the mechanism of hydrated Zn ions on the surface of sphalerite, PDOSs of bonding atoms after the adsorption of hydrated Zn ion are performed, with the results presented in Figures 8–10. The Fermi level's position is set to 0 eV. Significant chemical processes are usually reflected near the Fermi level.

The PDOSs of bonding atoms after the adsorption of $[Zn(H_2O)_5]^{2+}$ on the sphalerite (110) surface are shown in Figure 8. The mixing in the range −10.0 eV to −2.5 eV is mainly attributed to the $Zn_{b\text{-}1}$ 3d and S_7 3p states, which indicates that the bonding of $Zn_{b\text{-}1}$ and S_7 atoms have a strong covalent interaction. The antibonding interactions attributed by the $Zn_{b\text{-}1}$ 3p and S_7 3p states are mainly found in the conduction band at 0.4 eV~6.7 eV. In addition, the bonding atoms between $H_{b\text{-}1}$ and S_6, $H_{b\text{-}3}$ and S_3, and $H_{b\text{-}2}$ and S_8 have no effective overlap. The interaction between them is weak.

The PDOSs of bonding atoms after the adsorption of $[Zn(OH)(H_2O)_3]^{+}$ on the sphalerite (110) surface are shown in Figure 9. It is observed that the Zn_6 3d and $O_{c\text{-}1}$ 3p states show some activity, and their overlapping area are widely distributed in the range from −7.0 eV to 0 eV. The strong bonding interactions of Zn_6 and $O_{c\text{-}1}$ near the Fermi level are contributed to by the Zn_6 3d and $O_{c\text{-}1}$ 3p states. Besides, the PDOS of $H_{c\text{-}1}$1s and S_2 3s have a weak interaction at −12.9 eV to −11.4 eV. The PDOS of $H_{c\text{-}2}$1s and S_6 3s also have a weak interaction at −12.5 eV to −11.3 eV and −10.0 eV to −8.9 eV.

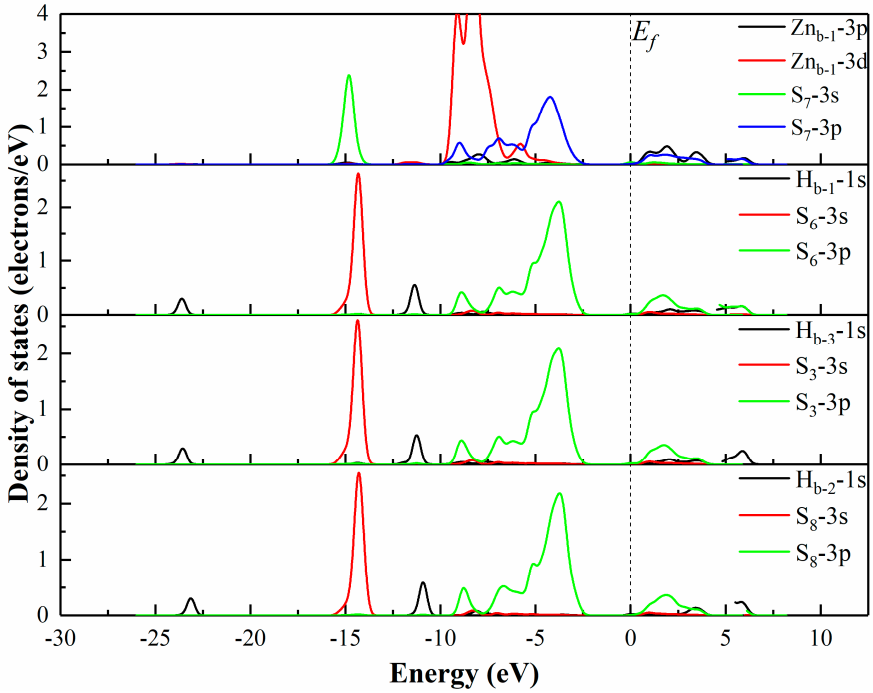


Figure 8. PDOSs of bonding atoms after the adsorption of $[Zn(H_2O)_5]^{2+}$ on the sphalerite (110) surface.

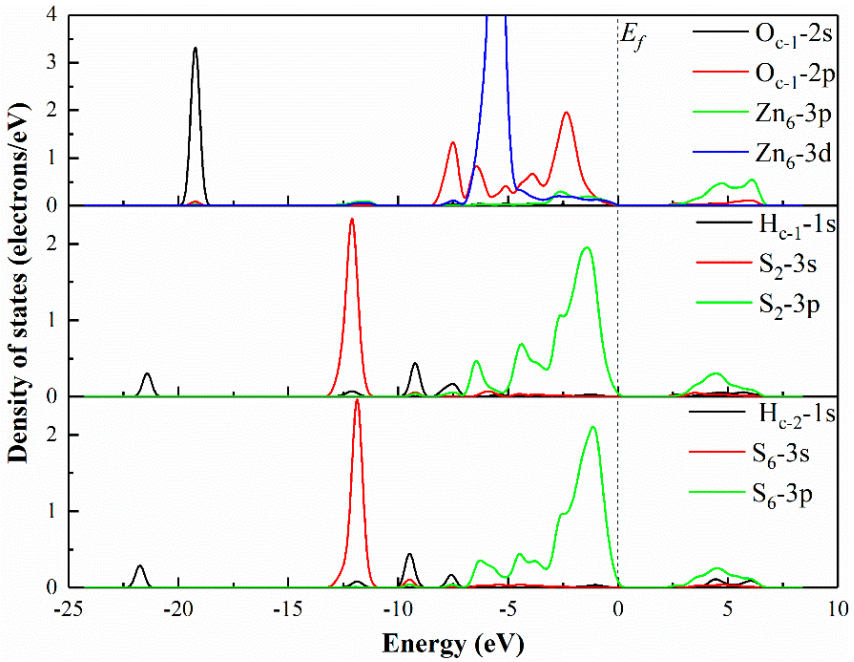


Figure 9. PDOS of bonding atoms after the adsorption of $[Zn(OH)(H_2O)_3]^{+}$ on the sphalerite (110) surface.

The PDOSs of bonding atoms after the adsorption of $[Zn(OH)_2(H_2O)_2]$ on the sphalerite (110) surface are shown in Figure 10. The PDOSs of Zn_6 3d and O_{d-1} 2p possess effective overlap at −6.5 eV to 0 eV. The PDOSs of Zn_7 3d and O_{d-2} 2p also display an effective overlap at the region from −6.5 eV to 0 eV. It shows that the interactions of Zn_6 with O_{d-1} and Zn_7 with O_{d-2} are very strong. However, the bonding atoms of H_{d-1}–S_2 and H_{d-2}–S_6 do not have an obvious overlap, suggesting their weak interaction.

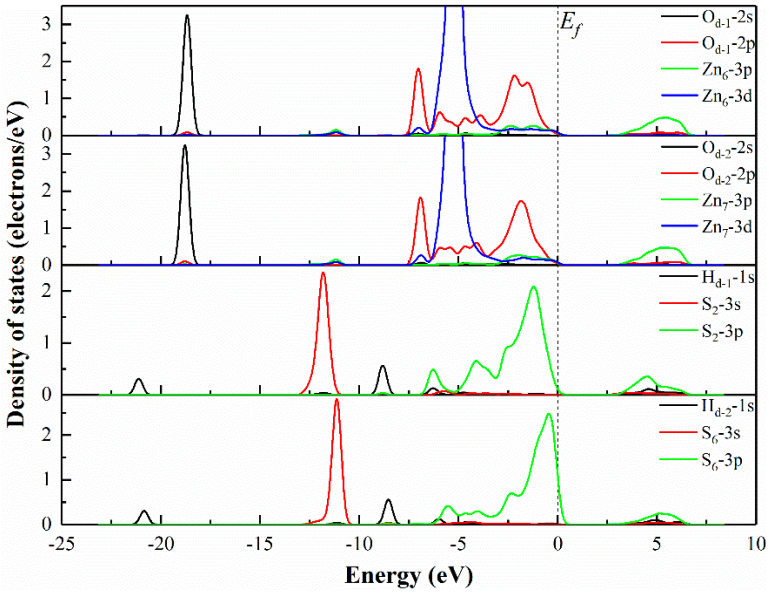


Figure 10. PDOS of bonding atoms after the adsorption of $[Zn(OH)_2(H_2O)_2]$ on the sphalerite (110) surface.

4. Conclusions

In order to better understand the depression mechanism of zinc ions on sphalerite in a flotation process, the influence of hydroxylation and hydration on the depression of zinc ions on sphalerite in a neutral aqueous solution was further discussed by using first-principle DFT calculation. Some conclusions are summarized as follows:

(1) The effective components of hydrated Zn ions adsorbed on a sphalerite (110) surface in a neutral aqueous solution are $[Zn(H_2O)_5]^{2+}$, $[Zn(OH)(H_2O)_3]^{+}$, and $[Zn(OH)_2(H_2O)_2]$, respectively.

(2) The adsorption energy values of Zn^{2+}, $[Zn(OH)]^{+}$ and $[Zn(OH)_2]$ on a sphalerite(110) surface are −17.4, −158.6, and −231.0 kJ/mol, respectively. After hydration, the adsorption energy values of $[Zn(H_2O)_5]^{2+}$, $[Zn(OH)(H_2O)_3]^{+}$, and $[Zn(OH)_2(H_2O)_2]$ on a sphalerite (110) surface are −144.5, −177.1, and −237.5 kJ/mol. The hydration could obviously promote the adsorption of Zn^{2+}, $[Zn(OH)]^{+}$, and $[Zn(OH)_2]$ on the surface of a sphalerite (110) surface.

(3) The adsorption mechanism of $[Zn(H_2O)_5]^{2+}$ on a sphalerite (110) surface is mainly ascribed to the hybridization of Zn 3d orbital in structure of $[Zn(H_2O)_5]^{2+}$ with surface S 3p orbital. Furthermore, the adsorption mechanism of $[Zn(OH)(H_2O)_3]^{+}$ and $[Zn(OH)_2(H_2O)_2]$ on the sphalerite (110) surface is primarily ascribed to the hybridization of surface Zn 3d orbital with 2p orbital of the O atom of the hydroxyl ligand.

This study helps us understand the effects of hydroxylation and hydration of metal ions on mineral flotation and the basic properties of the interface in mineral flotation.

Supplementary Materials: The following supporting information can be downloaded at: https://www.mdpi.com/article/10.3390/min13091113/s1, Figure S1: Optimized geometries of $[Zn(H_2O)_{1–8}]^{2+}$; Figure S2: Optimized geometries of $[Zn(OH)(H_2O)_{1–5}]^{+}$; Figure S3: Equilibrium geometries of $[Zn(OH)_2(H_2O)_{1–5}]$; Table S1: Structural parameters, adsorption energies (ΔE_{ad}, ΔG_{ad}), and successive water adsorption energies (ΔE_{sad}, ΔE_{sad}) of $[Zn(H_2O)_{1–8}]^{2+}$, $[Zn(OH)(H_2O)_{1–5}]^{+}$ and $[Zn(OH)_2(H_2O)_{1–4}]$; Table S2: Structural parameters, adsorption energies (ΔE_{ad}), and successive water adsorption energies (ΔE_{sad}) of $[Zn(H_2O)_{1–8}]^{2+}$, $[Zn(OH)(H_2O)_{1–5}]^{+}$ and $[Zn(OH)_2(H_2O)_{1–4}]$; Table S3: The adsorption energies of Zn^{2+}, $[Zn(OH)]^{+}$ and $Zn(OH)_2$ on the sphalerite (110) surface (kJ/mol); Table S4: The adsorption energies of $[Zn(H_2O)_5]^{2+}$, $[Zn(OH)(H_2O)_3]^{+}$ and $[Zn(OH)_2(H_2O)_2]$ on the sphalerite (110) surface (kJ/mol); Table S5: Hirshfeld charge populations of bonding atoms before and after $[Zn(H_2O)_5]^{2+}$, $[Zn(OH)(H_2O)_3]^{+}$ and $[Zn(OH)_2(H_2O)_2]$ adsorption; Table S6: Mulliken bond populations after the sphalerite adsorbed by $[Zn(H_2O)_5]^{2+}$, $[Zn(OH)(H_2O)_3]^{+}$ and $[Zn(OH)_2(H_2O)_2]$.

Author Contributions: C.Z.: Writing—original draft, Conceptualization, Methodology, Funding acquisition, Writing—review and editing. F.Z.: Writing—original draft, Formal analysis, Software, Writing—review and editing. S.L.: Visualization, Writing—review and editing, Validation, Investigation, Data curation. D.F.: Visualization, Writing—review and editing, Validation. X.R.: Visualization, Writing—review and editing, Validation. J.C.: Visualization, Writing—review and editing, Validation. J.W.: Supervision, Funding acquisition, Conceptualization, Writing—review and editing. Y.Z.: Visualization, Writing—review and editing, Validation. W.S.: Supervision, Conceptualization, Visualization, Funding acquisition, Writing—review and editing, Validation. All authors have read and agreed to the published version of the manuscript.

Funding: This work was financially supported by the National Key Research and Development Program of China (2022YFC2904503); The National Natural Science Foundation of China (Nos. 52074356, U20A20269, 22208252); The Science and Technology innovation Program of Hunan Province (2022RC1183); The Natural Science Foundation of Hunan Province (No. 2021JJ20069); Postdoctoral Research Foundation of China (No. 2020T130188); National 111 Project (No. B14034). The Fundamental Research Funds for the Central Universities of Central South University Project (No. 50621747). The Special fund for Carbon Peak and Carbon Neutrality science and technology innovation of Jiangsu Province in 2022 (BE2022601).

Data Availability Statement: The data presented is available in the article.

Acknowledgments: This work was carried out in part using hardware and/or software provided by the Computing Platform of Mineral Processing Computational Chemistry at School of Mineral Processing, Bioengineering of Central South University, and the High-Performance Computing Centers of Central South University, and Tianhe II supercomputer at the National Supercomputing Center in Guangzhou.

Conflicts of Interest: We declare that we have no financial and personal relationships with other people or organizations that can inappropriately influence our work, there is no professional or other personal interest of any nature or kind in any product, service and/or company that could be construed as influencing the position presented in, or the review of, the manuscript entitled.

References

1. Porento, M.; Hirva, P. Theoretical studies on the interaction of anionic collectors with Cu^{+}, Cu^{2+}, Zn^{2+} and Pb^{2+} ions. *Theor. Chem. Acc. Theory Comput. Model. (Theor. Chim. Acta)* **2002**, *107*, 200–205. [CrossRef]
2. Gao, Z.; Jiang, Z.; Sun, W.; Gao, Y. Typical roles of metal ions in mineral flotation: A review. *Trans. Nonferrous Met. Soc. China* **2021**, *31*, 2081–2101. [CrossRef]
3. Wang, H.; Wen, S.; Han, G.; Xu, L.; Feng, Q. Activation mechanism of lead ions in the flotation of sphalerite depressed with zinc sulfate. *Miner. Eng.* **2020**, *146*, 106132. [CrossRef]
4. Wang, H.; Wen, S.; Han, G.; Feng, Q. Effect of copper ions on surface properties of ZnSO4-depressed sphalerite and its response to flotation. *Sep. Purif. Technol.* **2019**, *228*, 115756. [CrossRef]
5. Luo, X.; Feng, B.; Wong, C.; Miao, J.; Ma, B.; Zhou, H. The critical importance of pulp concentration on the flotation of galena from a low grade lead–zinc ore. *J. Mater. Res. Technol.* **2016**, *5*, 131–135. [CrossRef]
6. Cao, Y.; Sun, L.; Gao, Z.; Sun, W.; Cao, X. Activation mechanism of zinc ions in cassiterite flotation with benzohydroxamic acid as a collector. *Miner. Eng.* **2020**, *156*, 106523. [CrossRef]
7. Peng, H.; Luo, W.; Wu, D.; Bie, X.; Shao, H.; Jiao, W.; Liu, Y. Study on the Effect of Fe3+ on Zircon Flotation Separation from Cassiterite Using Sodium Oleate as Collector. *Minerals* **2017**, *7*, 108. [CrossRef]
8. Yu, L.; Liu, Q.; Li, S.; Deng, J.; Luo, B.; Lai, H. Depression mechanism involving Fe3+ during arsenopyrite flotation. *Sep. Purif. Technol.* **2019**, *222*, 109–116. [CrossRef]
9. Zhang, H.; Zhang, F.; Sun, W.; Chen, D.; Chen, J.; Wang, R.; Han, M.; Zhang, C. The effects of hydroxyl on selective separation of chalcopyrite from pyrite: A mechanism study. *Appl. Surf. Sci.* **2023**, *608*, 154963. [CrossRef]
10. Luo, A.; Chen, J. Effect of hydration and hydroxylation on the adsorption of metal ions on quartz surfaces: DFT study. *Appl. Surf. Sci.* **2022**, *595*, 153553. [CrossRef]
11. Liu, X.; Lu, X.; Jan Meijer, E.; Wang, R. Hydration mechanisms of Cu^{2+}: Tetra-, penta- or hexa-coordinated? *Phys. Chem. Chem. Phys.* **2010**, *12*, 10801–10804. [CrossRef] [PubMed]
12. Liu, J.; Wang, Y.; Luo, D.; Zeng, Y. Use of ZnSO4 and SDD mixture as sphalerite depressant in copper flotation. *Miner. Eng.* **2018**, *121*, 31–38. [CrossRef]
13. Cui, Y.-F.; Jiao, F.; Qin, W.-Q.; Dong, L.-Y.; Wang, X. Synergistic depression mechanism of zinc sulfate and sodium dimethyl dithiocarbamate on sphalerite in Pb–Zn flotation system. *Trans. Nonferrous Met. Soc. China* **2020**, *30*, 2547–2555. [CrossRef]

14. Wei, Z.; Wang, H.; Xue, C.; Zeng, M. Selective depression of sphalerite by combined depressant $K_3[Fe(CN)_6]$, $ZnSO_4$, and Na_2CO_3 in Pb–Zn sulfide flotation separation. *Chem. Pap.* **2019**, *74*, 421–429. [CrossRef]
15. Wei, Q.; Dong, L.; Qin, W.; Jiao, F.; Qi, Z.; Feng, C.; Sun, D.; Wang, L.; Xiao, S. Efficient flotation recovery of lead and zinc from refractory lead-zinc ores under low alkaline conditions. *Geochemistry* **2021**, *81*, 125769. [CrossRef]
16. Luo, Y.; Ou, L.; Chen, J.; Zhang, G.; Xia, Y.; Zhu, B.; Zhou, H. Mechanism insights into the hydrated Al ion adsorption on talc (001) basal surface: A DFT study. *Surf. Interfaces* **2022**, *30*, 101973. [CrossRef]
17. Luo, Y.; Ou, L.; Chen, J.; Zhang, G.; Xia, Y.; Zhu, B.; Zhou, H. Insights into the adsorption performance and mechanism of hydrated Ca ion on talc (0 0 1) basal surface from DFT calculation. *Int. J. Min. Sci. Technol.* **2022**, *32*, 887–896. [CrossRef]
18. Liu, J.; Wang, Y.; Luo, D.; Zeng, Y.; Wen, S.; Chen, L. DFT study of SDD and BX adsorption on sphalerite (1 1 0) surface in the absence and presence of water molecules. *Appl. Surf. Sci.* **2018**, *450*, 502–508. [CrossRef]
19. Segall, M.; Lindan, P.J.; Probert, M.a.; Pickard, C.J.; Hasnip, P.J.; Clark, S.; Payne, M. First-principles simulation: Ideas, illustrations and the CASTEP code. *J. Phys. Condens. Matter* **2002**, *14*, 2717. [CrossRef]
20. Skinner, B.J. Unit-cell edges of natural and synthetic sphalerites. *Am. Mineral. J. Earth Planet. Mater.* **1961**, *46*, 1399–1411.
21. Perdew, J.P.; Burke, K.; Wang, Y. Generalized gradient approximation for the exchange-correlation hole of a many-electron system. *Phys. Rev. B* **1996**, *54*, 16533. [CrossRef] [PubMed]
22. Luo, Y.J.; Ou, L.M.; Chen, J.H.; Zhang, G.F.; Xia, Y.Q.; Zhu, B.H.; Zhou, H.Y. Hydration mechanisms of smithsonite from DFT-D calculations and MD simulations. *Int. J. Min. Sci. Technol.* **2022**, *32*, 605–613. [CrossRef]
23. Bucko, T.; Lebegue, S.; Hafner, J.; Angyan, J.G. Tkatchenko-Scheffler van der Waals correction method with and without self-consistent screening applied to solids. *Phys. Rev. B* **2013**, *87*, 064110. [CrossRef]
24. Wright, K.; Watson, G.W.; Parker, S.C.; Vaughan, D.J. Simulation of the structure and stability of sphalerite (ZnS) surfaces. *Am. Mineral.* **1998**, *83*, 141–146. [CrossRef]
25. Chen, J.H.; Chen, Y.; Li, Y.Q. Effect of vacancy defects on electronic properties and activation of sphalerite (110) surface by first-principles. *Trans. Nonferrous Met. Soc. China* **2010**, *20*, 502–506. [CrossRef]
26. Steele, H.M.; Wright, K.; Hillier, I.H. A quantum-mechanical study of the (110) surface of sphalerite (ZnS) and its interaction with Pb2+ species. *Phys. Chem. Miner.* **2003**, *30*, 69–75. [CrossRef]
27. Zhang, H.; Sun, W.; Zhang, C.; He, J.; Chen, D.; Zhu, Y. Adsorption performance and mechanism of the commonly used collectors with Oxygen-containing functional group on the ilmenite surface: A DFT study. *J. Mol. Liq.* **2022**, *346*, 117829. [CrossRef]
28. Zhang, H.; Sun, W.; Zhu, Y.; He, J.; Chen, D.; Zhang, C. Effects of the Goethite Surface Hydration Microstructure on the Adsorption of the Collectors Dodecylamine and Sodium Oleate. *Langmuir* **2021**, *37*, 10052–10060. [CrossRef]
29. Wang, X.; Liu, R.; Ma, L.; Qin, W.; Jiao, F. Depression mechanism of the zinc sulfate and sodium carbonate combined inhibitor on talc. *Colloids Surf. A Physicochem. Eng. Asp.* **2016**, *501*, 92–97. [CrossRef]
30. Hartmann, M.; Clark, T.; van Eldik, R. Hydration and Water Exchange of Zinc(II) Ions. Application of Density Functional Theory. *J. Am. Chem. Soc.* **1997**, *119*, 7843–7850. [CrossRef]
31. Mhin, B.J.; Lee, S.; Cho, S.J.; Lee, K.; Kim, K.S. $Zn(H_2O)^{2+}{}_6$ is very stable among aqua-Zn(II) ions. *Chem. Phys. Lett.* **1992**, *197*, 77–80. [CrossRef]
32. Frisch, M.; Trucks, G.; Schlegel, H.; Scuseria, G.; Robb, M.; Cheeseman, J.; Scalmani, G.; Barone, V.; Mennucci, B.; Petersson, G. *Gaussian 09*; Gaussian, Inc.: Wallingford, CT, USA, 2009.
33. Remya, K.; Suresh, C.H. Which density functional is close to CCSD accuracy to describe geometry and interaction energy of small noncovalent dimers? A benchmark study using Gaussian09. *J. Comput. Chem.* **2013**, *34*, 1341–1353. [CrossRef]
34. Chen, Y.; Liu, X.; Chen, J. Steric hindrance effect on adsorption of xanthate on sphalerite surface: A DFT study. *Miner. Eng.* **2021**, *165*, 106834. [CrossRef]
35. Guo, X.; Li, L.; Liu, Z.; Yu, D.; He, J.; Liu, R.; Xu, B.; Tian, Y.; Wang, H.-T. Hardness of covalent compounds: Roles of metallic component and d valence electrons. *J. Appl. Phys.* **2008**, *104*, 023503. [CrossRef]

Disclaimer/Publisher's Note: The statements, opinions and data contained in all publications are solely those of the individual author(s) and contributor(s) and not of MDPI and/or the editor(s). MDPI and/or the editor(s) disclaim responsibility for any injury to people or property resulting from any ideas, methods, instructions or products referred to in the content.